


# Combined ROS Responsive Polydopamine-Coated Berberine Nanoparticles Effective Against Ulcerative Colitis in Mouse Model

Chenqi Chang<sup>1</sup>, Heng Liu<sup>2</sup>, Xiaotong Li<sup>2</sup>, Dandan Song<sup>1</sup>, Yue Liu<sup>1</sup>, Chang Lu<sup>1</sup>, Yu Zhen<sup>1</sup>, Ying Chen<sup>1</sup>, Jinguo Xu<sup>1</sup>, Weidong Li<sup>1</sup>, Xiaobin Jia<sup>3</sup>, Zhipeng Chen<sup>1</sup>, Rui Chen<sup>1</sup> 

<sup>1</sup>School of Pharmacy, Nanjing University of Chinese Medicine, Nanjing, 210023, People's Republic of China; <sup>2</sup>Yunnan Provincial Key Laboratory of Entomological Biopharmaceutical R&D, College of Pharmacy, Dali University, Dali, 671003, People's Republic of China; <sup>3</sup>School of Traditional Chinese Pharmacy, China Pharmaceutical University, Nanjing, 211198, People's Republic of China

Correspondence: Rui Chen; Zhipeng Chen, Email [chenrui@njucm.edu.cn](mailto:chenrui@njucm.edu.cn); [czpcpu2000@hotmail.com](mailto:czpcpu2000@hotmail.com)

**Introduction:** Enhancing the efficacy of berberine (BBR) in the treatment of ulcerative colitis (UC) through the development of dopamine-coated berberine nanoparticles (PDA@BBR NPs) with ROS-responsive and adhesive properties.

**Methods:** Berberine nanoparticles (BBR NPs) were synthesized using the nonsolvent precipitation method, and their surfaces were coated with polydopamine (PDA) through oxidative polymerization. The PDA@BBR NPs were characterized by transmission electron microscopy (TEM), size analysis, and zeta potential analysis. Drug loading and encapsulation efficiency were analyzed using fluorescence spectroscopy. The responsiveness of these nanoparticles to reactive oxygen species (ROS) was assessed in vitro, while their adhesive properties and therapeutic efficacy on UC were evaluated in vivo.

**Results:** Physicochemical property studies showed that PDA coated BBR NPs nanoparticles have good dispersion and stability. In vitro results showed that PDA@BBR NPs could prolong the retention time of the drug at the colonic site and could realize the gradual drug release under ROS environment. In addition, animal studies showed that PDA@BBR NPs exhibited significant anti-inflammatory effects on DSS-induced colitis and effectively reduced intestinal mucosal damage.

**Conclusion:** PDA@BBR NPs are ROS-responsive nanoparticles that adhere well and have a high drug loading capacity. They have shown therapeutic effects in mice with UC, indicating that this formulation may be a promising treatment option.

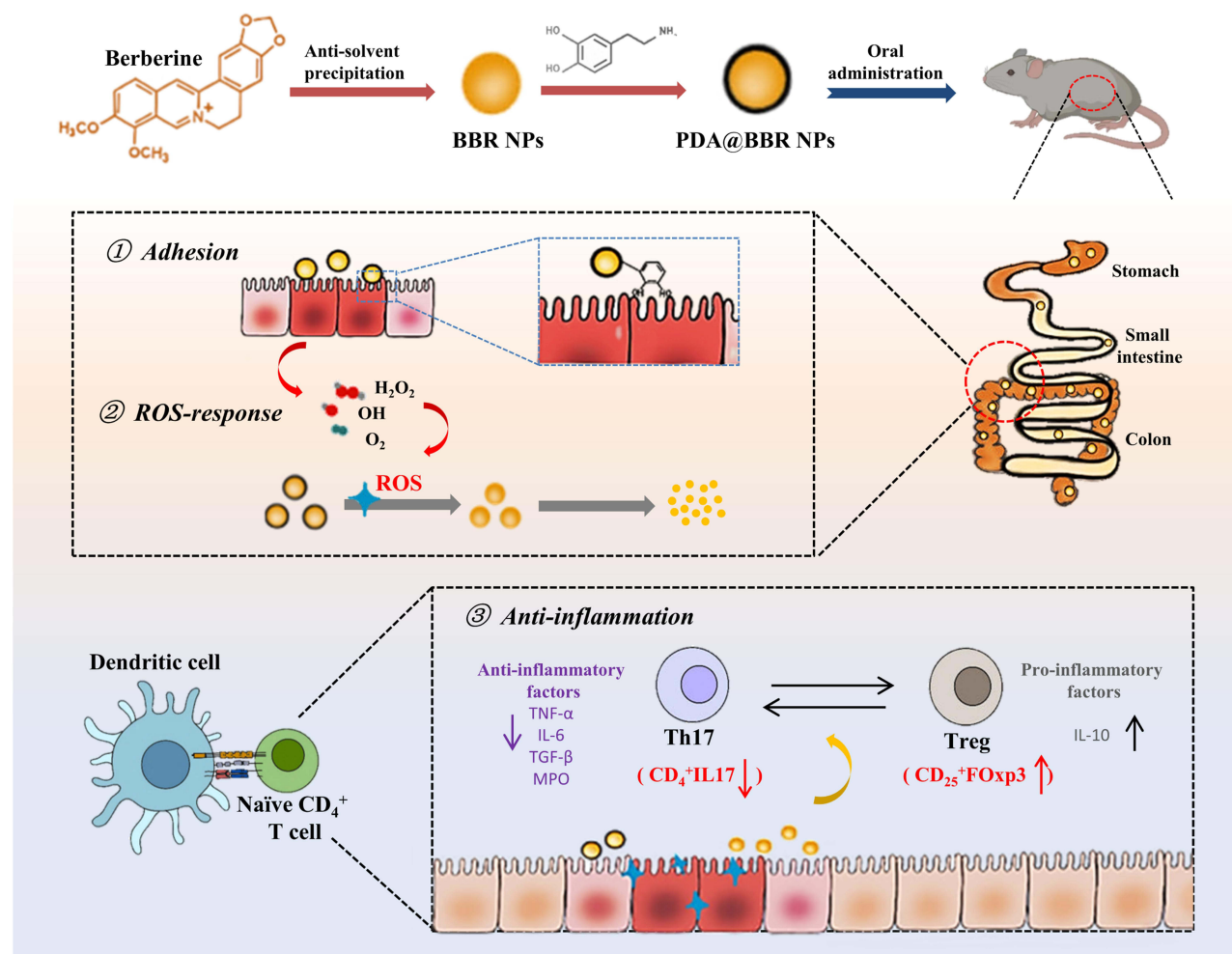
**Keywords:** berberine, polydopamine, ROS-responsive, adhesion retention, ulcerative colitis

## Introduction

Ulcerative colitis (UC) is a chronic and complex inflammatory bowel disease. Clinically, it manifests as diarrhea, mucopurulent and bloody stools, urgency, and severity, with a tendency for recurrent episodes.<sup>1</sup> The global incidence and prevalence of UC have been increasing in recent years, but the underlying causes and mechanisms remain unclear. Currently, there are two main methods for treating UC: surgical treatment and drug therapy. Surgical treatment is mainly targeted at UC patients with recurrent bleeding, intestinal perforation, and toxic megacolon.<sup>2,3</sup> Drug therapy includes aminosalicylates, corticosteroids, probiotics, and biologics. However, these treatments are often limited by a single treatment mechanism and the potential for adverse or toxic side effects. Additionally, the pathological characteristics of recurrent diarrhea in UC necessitate frequent and multiple drug administrations, which place greater demands on the therapeutic drugs for UC, especially those with long-term efficacy. Therefore, the development of safe, low-toxicity, multi-site-targeting and prolonged drug retention time candidate drugs is crucial.

In the local lesions of UC patients, the concentration of reactive oxygen species (ROS) significantly increases, being 10 to 100 times higher than in healthy individuals.<sup>4</sup> This excessive oxidative stress is a characteristic of UC lesions.<sup>5,6</sup> The safety of drug carriers and the release kinetics of drugs under oxidative-reductive stimuli are important considerations for

## Graphical Abstract



drug delivery systems responsive to ROS.<sup>7,8</sup> Therefore, it is urgently necessary to find a material that is safe, effective, and capable of achieving ROS-specific degradation in order to develop a colon-targeted drug delivery system.

Dopamine (DA) contains a large number of phenolic hydroxyl and amino groups, and can form polydopamine (PDA) through both covalent and non-covalent bonds under alkaline conditions. Due to the unique ortho-quinone functional group in DA, it can adhere to the intestinal mucosa, prolonging the retention time of the drug, and is commonly used to prepare adhesive hydrogels.<sup>9,10</sup> PDA has strong wet adhesion and can adhere more firmly to the small intestinal mucosa, thereby addressing the issue of low drug bioavailability caused by UC-related diarrhea. In addition, PDA also possesses ROS-responsive degradation and ROS scavenging properties, enabling local drug targeting through ROS response.<sup>11–13</sup>

Berberine (BBR), an isoquinoline alkaloid extracted from the plants *Coptidis Rhizoma* and *Phellodendri Chinensis Cortex*,<sup>14</sup> has been shown to possess various pathological effects, including anti-malarial, anti-arrhythmic, anti-hyperglycemic, antioxidant, antimicrobial, and anticancer effects. It is commonly used clinically as a major drug for treating enteritis.<sup>15,16</sup> Despite its clinical potential, BBR suffers from a low intestinal absorption rate and hepatic first-pass effect, resulting in poor bioavailability (5%) and requiring frequent or high-dose administration. This greatly affects patient compliance and acceptance.<sup>17</sup> Therefore, it is necessary to develop new oral formulations of berberine to improve the condition of UC.

We utilized the multiple properties of PDA to prepare an intelligent delivery system for BBR, called PDA@BBR NPs, and studied their characteristics, responsiveness to ROS, adhesion, and in vivo therapeutic effects on UC. We first

explored the reactivity of PDA@BBR NPs to ROS in vitro and their adhesion in vivo. The study focused on the challenges related to BBR, such as its low solubility, poor bioavailability, and potential gastrointestinal irritation. Furthermore, our in vivo experiments demonstrated that PDA@BBR NPs effectively improved UC and may be associated with regulating the balance of Th17/Treg cells. These findings provide valuable evidence for the development of formulations targeting inflammation and adhesion in the gastrointestinal tract. Additionally, they contribute to advancing the local administration of anti-inflammatory drugs.

## Materials and Methods

### Materials

Berberine (purity  $\geq 98\%$ ) was purchased from Shanghai Yuanye Biotechnology Co. (China). Dopamine hydrochloride was purchased from Sigma-Aldrich (St. Louis, MO, USA). CY7.5 NHS ester was purchased from Lumiprobe (USA). Tris-base (purity  $\geq 99\%$ ) was purchased from Shanghai Yuanye Biotechnology Co (China). Human colorectal adenocarcinoma cells (Caco-2) were purchased from the Cell Bank of the Chinese Academy of Sciences (China). Fetal bovine serum was purchased from Nanjing Nuoweizan Co., Ltd. (China), DEAE medium, trypsin, and streptomycin-penicillin solution were purchased from Wuhan Seville Biotechnology Co. (China). Lipopolysaccharide and Dapi were purchased from Beyotime Biotechnology Co. (China). Mesalazine sodium capsules were purchased from Zhejiang Huarun Sanjiu Zhongyi Pharmaceutical Co (China). Dextran sodium sulfate (DSS) was purchased from Shenzhen Regent Biochemical Technology Co (China). Cryptohematology kits were purchased from Beijing Regent Bio-technology Co (China). TNF- $\alpha$ , IL-6, MPO, IL-10, TGF- $\beta$  kits were purchased from Shanghai Yuanquan Biotechnology Center (China).

### Animals

C57BL/6 male mice, 18–22 g, were purchased from Chengdu Dashuo Laboratory Animal Company (Sichuan, China; SYXK (Shen) 2018 –0002). They were housed in the IVC system of the Animal Experiment Center of Dali University at a temperature of 20–25°C, humidity of 40–70%, and 12 h of alternating light and dark. All animal experiments were approved by the Animal Ethics Committee of Dali University (2023-PZ-193) and performed in strict accordance with the national standards of the People's Republic of China, "Guidelines for Ethical Review of Laboratory Animal Welfare" (GB/T 35892–2018) and "Guidelines for the Review of Humane Endpoints in Animal Experiments" (RB/T 173–2018).

## Synthesis of Polydopamine-Coated Berberine Nanoparticles

### Synthesis of Berberine Nanoparticles

A stock BBR solutions were prepared by dissolving 25.0 mg of BBR into 10 mL of anhydrous ethanol to obtain a stock solution at the concentration of 2.5 mg·mL<sup>-1</sup>. The stock solution was stored at -20°C and used at ambient temperature. To prepare carrier-free Berberine nanoparticle (BBR NPs), the BBR solution (100  $\mu$ L) was rapidly injected into distilled water (10 mL) and sonicated for 5 min to obtain BBR NPs with concentration from 10.0 to 100.0  $\mu$ g·mL<sup>-1</sup> were obtained.

### Synthesis of Polydopamine-Coated Berberine Nanoparticles

BBR NPs were prepared as described above. Aqueous dopamine hydrochloride (PDA) (0.2 mg·mL<sup>-1</sup>) and Tris base solution (6 mg·mL<sup>-1</sup>) were added into the solution of BBR NP sequentially to obtain an alkaline environment at pH=8.5. Then, the Polydopamine-coated Berberine nanoparticles (PDA@BBR NPs) suspension was obtained by reacting for 6 h under magnetic stirring at room temperature. Finally, the product was purified by centrifugation at 13,000 r·min<sup>-1</sup> for 15 min and washed three times with distilled water to remove the unloaded BBR.

### Synthesis of Polydopamine-Coated Berberine Nanoparticles with Different Coating Thickness

The coating thickness of PDA was varied by changing the reaction time (5–7 h) or the concentration of PDA (0.1–0.5 mg·mL<sup>-1</sup>) to obtain PDA@BBR NPs with controllable coating thickness.

## Characterizations of Berberine Nanoparticles and Polydopamine-Coated Berberine Nanoparticles

### Measurement of Particle Size and Zeta Potential of Nanoparticles

The particle size and zeta potential of BBR NPs and PDA@BBR NPs aqueous dispersions were measured by a Malvern-Zetasizer ZS-90 dynamic light scattering (DLS) instrument. All samples were measured at 25 °C and repeated three times.

### Morphological Observation of Nanoparticles

The morphology of nanoparticles with different coating thicknesses was observed by transmission electron microscopy (TEM, H-7800, HITACHI, Tokyo, Japan). The measurements were performed at an accelerating voltage of 80 KV, and the samples were prepared by dropping the NPs solution onto the copper grids and staining them with 2% uranyl acetate.

### Spectral Characteristics of Nanoparticles

Investigation of the spectral properties of BBR NPs and PDA@BBR NPs using UV-vis (Unico UV-4800, China) and fluorescence spectra (PerkinElmer LS45, JPN).

### Determination of Encapsulation Efficiency and Loading Capacity

The fluorescence intensities of different concentrations of series of berberine (Ex = 352 nm, Em = 553 nm) were measured by fluorescence spectrophotometer, and the standard curves were obtained to calculate the encapsulation efficiency and loading capacity of nanoparticles, and the supernatant was collected and repeated three times.

Measurement conditions: excitation slit: 5 nm, emission slit: 5 nm; response value: 1.2; signal gain:  $\times 0.1$ ; scan extension: 1; integration time 1.2; scan speed  $300 \text{ nm} \cdot \text{min}^{-1}$ ; quartz colorimetric cup: 1 cm; excitation wavelength 352 nm; emission wavelength: 553 nm;

The dose of added drug subtracted by that in the supernatant was the dose of BBR in PDA@BBR NPs. EE and LC were calculated as follows:

$$\text{EE (\%)} = (M - M1)/M \times 100\%$$

$$\text{LC (\%)} = (M - M1)/W \times 100\%$$

M1: the amount of free drug in supernatant; M: total amount of added drug; W: mass of NPs after removal of free drug.

## Stability of Berberine Nanoparticles and Polydopamine-Coated Berberine Nanoparticles

### Time Stability

The BBR NPs and PDA@BBR NPs were placed at 25°C in a light-proof environment. The particle size was measured at 0, 1, 3, 5 and 7 days and repeated three times.

### Media Stability

PDA@BBR NPs were placed in PBS at pH=2 or pH=11, anhydrous ethanol, 30% hydrogen peroxide for 24 h at 25°C, protected from light, then the supernatant was centrifuged at  $13,000 \text{ r} \cdot \text{min}^{-1}$  for 15 min and the drug dissolution rate was determined by fluorescence spectrophotometer (Ex = 352 nm, Em = 553 nm) and repeated three times.

## ROS-Stimulus Response Release of Polydopamine-Coated Berberine Nanoparticles

### Time-Dependent Release

The same concentration of PDA@BBR NPs, dissolved in 30% hydrogen peroxide solution, were observed by transmission electron microscopy and Malvern particle size meter at 0, 1, 6 and 24 h of reaction for morphological changes and particle size changes of nanoparticles and repeated three times.

### ROS-Dependent Release

The same concentration of PDA@BBR NPs were dissolved in 30%, 3% and 0.3% hydrogen peroxide solutions, and 1 mL of the solution was taken at 0.5, 1, 2, 4, 6, 8, 12, 24 and 48 h of the reaction, respectively, with  $13,000 \text{ r} \cdot \text{min}^{-1}$  high-speed



centrifugation for 15 min, and the supernatant was taken to measure the fluorescence intensity to obtain the dissolution of the drug and repeated three times.

### Coating Thickness-Dependent Release

PDA@BBR NPs with different coating thicknesses were dissolved in 3% hydrogen peroxide solution, and 1 mL of the solution was taken at 0.5, 1, 2, 4, 6, 8, 12, 24 and 48 h of the reaction, respectively, and centrifuged at  $13,000\text{ r}\cdot\text{min}^{-1}$  for 15 min at high speed, and the supernatant was taken to measure the fluorescence intensity to obtain the dissolution of the drug and repeated three times.

### Cell Imaging

Human colorectal adenocarcinoma-derived intestinal epithelial cells (Caco-2) were grown in DMEM supplemented with 20% fetal bovine serum, and 50 U/mL penicillin-streptomycin. Caco-2 cells were seeded in 6-well culture plates at a concentration of  $1\times 10^5$  cells/well and incubated for 24 hours to allow cells adhesion. Lipopolysaccharide (LPS) ( $500\text{ ng}\cdot\text{mL}^{-1}$ ) was then added to stimulate the cells for 12 hours, except for the control group. PDA@BBR NPs ( $10\text{ mM}$ ) were administered, and the cells were stained with Dapi for 10 minutes in the dark. Cell imaging was observed using a fluorescence microscope at 1, 6, 12, and 24 hours. BBR exhibited green fluorescence under excitation at 324 nm and emission at 553 nm, while Dapi exhibited blue fluorescence under excitation at 360 nm and emission at 488 nm.

## In vivo Adhesion of Polydopamine-Coated Berberine Nanoparticles

### Synthesis of Cy7.5 Labeled Polydopamine-Coated Berberine Nanoparticles

First, 9 mL of water and 1 mL of PDA@BBR NPs were added to a 50 mL centrifuge tube and mixed well. Then, 1 mg of Cy7.5 was added and mixed well. The solution gradually turned blue-green. After the reaction under magnetic stirring for 1 h, the solution was centrifuged at  $13,000\text{ r}\cdot\text{min}^{-1}$  for 15 min. The lower layer was washed 3 times with water and dispersed in 1 mL of water to obtain CY7.5-PDA@BBR NPs.

### In vivo Imaging and Assay in Mice

To assess the distribution of different agents in each tissue after oral administration, real-time tissue distribution was imaged in mice. After 7 days of acclimatization, C57BL/6 mice were randomly divided into three groups: Cy7.5, Cy7.5-NPs, and Cy7.5-NPs-UC (3% DSS-induced UC). After oral administration at 2, 6, 12, and 24 hours, the mice were euthanized. The fluorescence intensity of the mice was observed using the Maestro in vivo fluorescence imaging system (CRi Inc. Woburn, MA) and Image J 1.48 software (National Institutes of Health) to evaluate the distribution of the drug in various tissues.

## In vivo Therapeutic Evaluation

### Animals

A total of 48 C57BL/6 mice were randomly selected, with 6 mice used as the normal group, and the remaining mice were optimized based on the DSS-induced UC model in previous literature.<sup>18</sup> The specific method is as follows: the mice were first injected with a 3% DSS solution for 4 days, followed by an injection of a 2% DSS solution for 6 days to establish the UC mouse model. The modeling method for the normal group was the same, with modeling reagents added to distilled water. The successfully modeled mice were randomly divided into four groups: the model group, mesalazine group ( $200\text{ mg}\cdot\text{kg}^{-1}$ ), BBR group ( $20\text{ mg}\cdot\text{kg}^{-1}$ ), and PDA@BBR NPs group ( $30\text{ mg}\cdot\text{kg}^{-1}$ ), with  $n=6$  in each group. The normal group and model group were given oral gavage of normal saline, while the remaining drug groups were given the corresponding drugs orally once a day for 7 consecutive days.

### Conventional Indices

During the experiment, the changes in the body weight, diet and water intake, voluntary activity, and mental state of the mice were recorded daily. According to Table 1, the health status of the mice was comprehensively evaluated using the Disease Activity Index (DAI), which mainly included weight loss, stool shape, and fecal occult blood. On the last day, the mice were anesthetized and euthanized, and then the colon and major organs (heart, liver, spleen, lungs, and kidneys)

**Table I** Scoring Standard of Histopathology

Epithelial Cells	Inflammatory Cells Infiltration	Score
Normal pattern	No infiltration	0
Loss of cup cells	Infiltration to crypt basal layer	1
Large loss of cup cells	Infiltration to the mucosal basal layer	2
Loss of crypt cells	Infiltration deep into the muscular layer of the mucosa, accompanied by mucosal	3
Large loss of crypt cells	Infiltration reaches the submucosal layer	4

were harvested. The condition of the colon was observed, and the lengths were compared between the groups. The weight of the spleen was measured and compared between the groups.

Organ index= Organ mass (mg) / mouse body weight (g)

### Histopathological Score (HS)

Obtain colon tissue samples from mice of different groups, fix them with 4% paraformaldehyde, and then proceed with dehydration, paraffin embedding, sectioning, staining, and preparation of He slides. Observe the pathological sections under a light microscope and score the colon histological score (HS) according to the standards set by Ekström GM and others.

### Enzyme-Linked Immunosorbent Assay (ELISA)

During the test, colon tissue is taken and subjected to gradient freezing and thawing at  $-20^{\circ}\text{C}$  and  $4^{\circ}\text{C}$ . A 10% (W/V) homogenate is prepared using pre-chilled PBS, and then centrifuged at  $3500\text{ r}\cdot\text{min}^{-1}$  for 10 minutes at  $4^{\circ}\text{C}$ . The supernatant is collected and the levels of TNF- $\alpha$ , IL-6, IL-10, MPO, and TGF- $\beta$  in the colon tissue are strictly tested according to the instructions of the relevant reagent kit.

### Changes of T-Lymphocyte Subpopulations in the Spleen of Mice

The spleen of the mouse was removed under aseptic conditions, washed with ice-cold saline, and quickly weighed. The spleen was then minced and filtered to obtain splenocytes. Red blood cells were lysed and the cells suspension was prepared, then the cells concentration was calculated and adjusted to  $1\times 10^7\text{ cells}\cdot\text{mL}^{-1}$ . Antibodies were added according to the antibody instructions, stained, and subjected to flow cytometry analysis.

## Data Processing and Statistical Analysis

All data were analyzed and processed using SPSS 20.0. The experimental data for each group were represented as mean  $\pm$  standard deviation. Data that followed a normal distribution were analyzed using one-way analysis of variance, with intergroup comparisons conducted using LSD test. Data that did not follow a normal distribution were analyzed using Tamhane's T2 method. Continuous data from repeated measurements were analyzed using repeated measures analysis of variance. Differences were considered significant at  $*p<0.05$  and highly significant at  $***p<0.001$ . Graphs were created using GraphPad Prism 9.5.

## Results

### Synthesis and Characterization of Berberine Nanoparticles

In comparison to BBR aqueous solution, BBR NPs exhibit a significant Tyndall effect, with a clearly visible light path (Figure 1A). As shown in the TEM image in Figure 1B, when the BBR concentration is  $50\text{ }\mu\text{g}\cdot\text{mL}^{-1}$ , BBR NPs appear as irregular nanospheres with diameters ranging from 50 to 100 nm. Particle size was monitored by DLS analysis at BBR NPs concentrations ranging from 10 to  $100\text{ }\mu\text{g}\cdot\text{mL}^{-1}$ . The measured hydrodynamic diameter of the nanoparticles ranged from 138.6 to 338.9 nm, with a polydispersity index (PDI) of 0.45 to 0.68 (Figure 1C). Notably, a BBR concentration of  $50\text{ }\mu\text{g}\cdot\text{mL}^{-1}$ , the nanoparticles exhibited the smallest size ( $138.6\pm 10.9\text{ nm}$ ) and the lowest PDI ( $0.45\pm 0.13$ ). At this concentration, the absolute value of the zeta potential reached its peak ( $-14.7\pm 2.0\text{ mV}$ ), indicating the highest stability

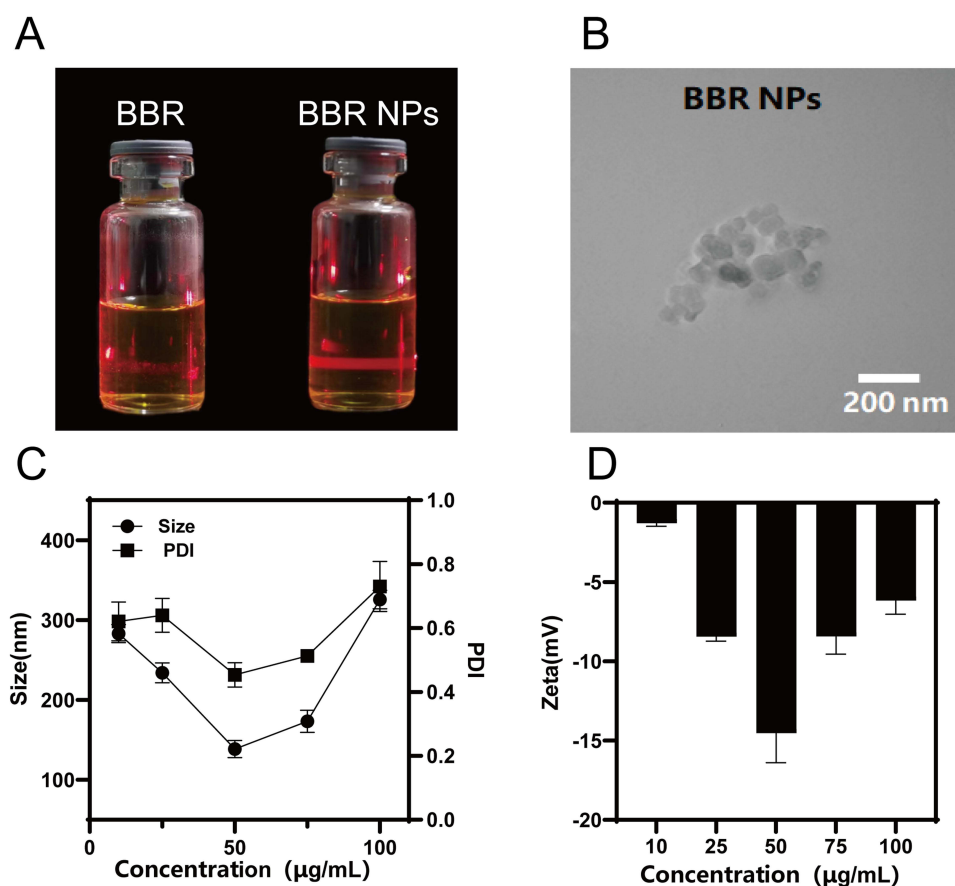


**Figure 1** Characteristics of BBR NPs. (A) Tyndall effect of BBR solution and BBR NP; (B) TEM images of BBR NPs; (C) Changes in particle size, PDI and (D) Zeta potential of BBR NPs at different BBR concentrations.

of the nanoparticles (Figure 1D). As observed in the TEM images, as the BBR concentration increases, BBR NPs become unstable and prone to aggregation. Therefore, it is necessary to find a method to maintain the stability of BBR NPs in practical applications.

## Preparation and Characterization of Polydopamine-Coated Berberine Nanoparticles

Under weak alkaline conditions, dopamine (DA) is easily oxidized and polymerized into polydopamine (PDA).<sup>19</sup> PDA can be conveniently used as a coating on the surface of BBR NPs. As shown in Figure 2A, after coating with PDA, the yellow color of the BBR NPs solution turns black, indicating successful coating. TEM analysis shows that PDA@BBR NPs have a regular spherical shape with a smooth and complete surface coating, measuring approximately 80 nm in diameter (Figure 2B). The hydrodynamic size of BBR NPs is  $138.6 \pm 10.9$  nm, with a polydispersity index (PDI) of 0.501. After coating with PDA, the hydrodynamic size of BBR NPs slightly increases to  $181.2 \pm 15.1$  nm, and the PDI decreases to 0.062, indicating uniform distribution (Figure 2C). The zeta potential of BBR NPs changes from  $-14.7 \pm 2.0$  mV to  $-38.5 \pm 0.26$  mV after coating with PDA, indicating improved dispersibility and stability (Figure 2D). Compared with the TEM results, DLS results show a slight increase in size and improved dispersibility. This difference can be attributed to the different sample preparation methods of the two detection techniques. In the DLS method, the nanoparticles are dispersed in the aqueous phase, which may cause the observed results to differ. TEM is performed after the nanoparticles are dried, which may lead to shrinkage and aggregation of the nanoparticles after water evaporation.

Further DLS measurements revealed a positive correlation between the thickness of the outer shell of the coating and factors such as reaction time and dopamine concentration (Figure 2E and F). This indicates that a thicker outer shell can

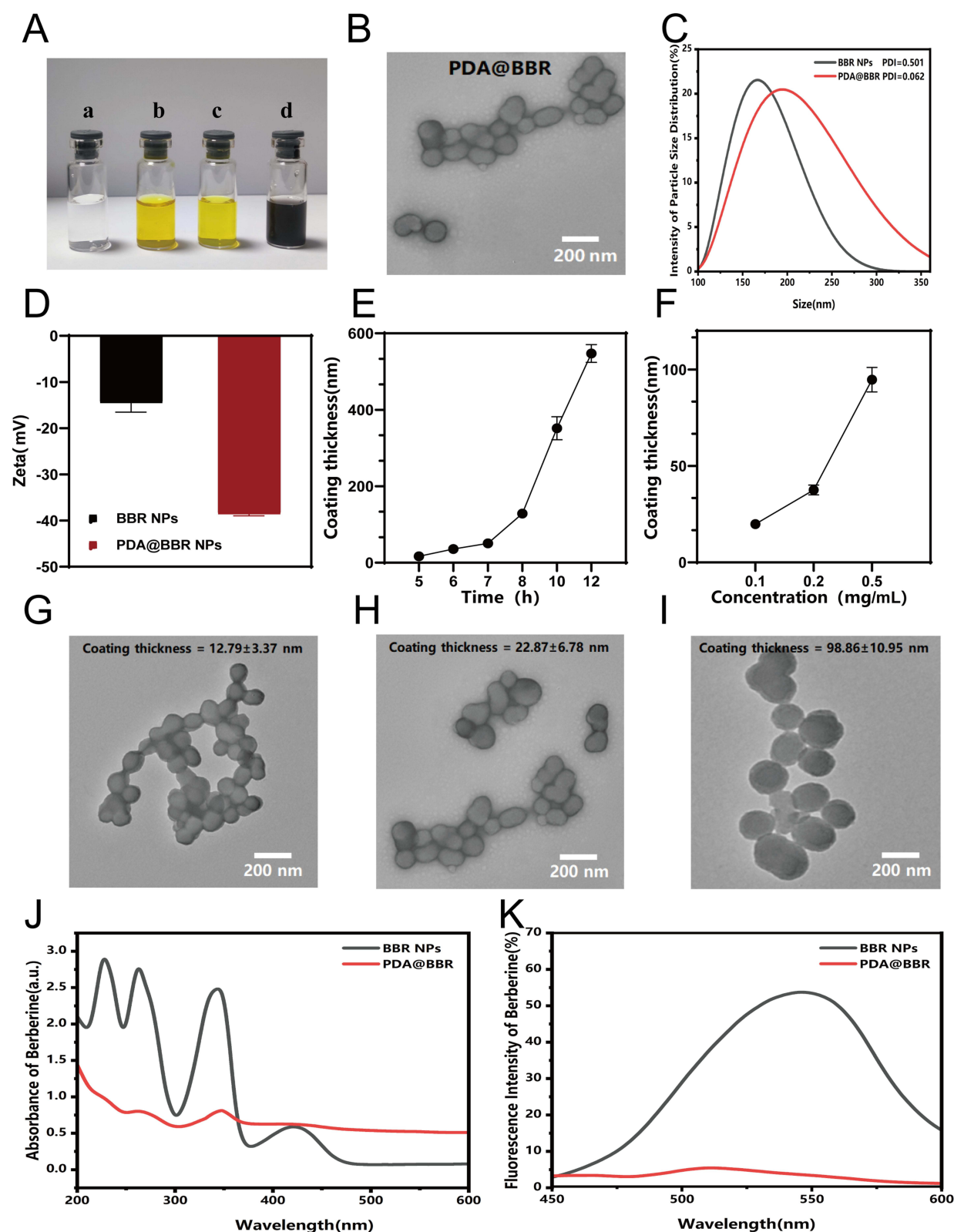


**Figure 2** Physical properties of PDA@BBR NPs. (A) Solution appearance for different samples; (a) H<sub>2</sub>O; (b) BBR; (c) BBR NPs; (d) PDA@BBR NPs; (B) TEM imaging of PDA@BBR NPs; (C) Intensity of particle size distribution of BBR and PDA@BBR NPs; (D) Zeta potential of BBR NPs and PDA@BBR NPs; (E) Variation of coating thickness of PDA@BBR NPs at different reaction times (5–12 hours); (F) Variation of coating thickness of PDA@BBR NP at different reaction concentrations (0.1–0.5 mg mL<sup>-1</sup>); (G) TEM images of PDA @ BBR NPs prepared from 0.1 mg mL<sup>-1</sup> PDA; (H) TEM images of PDA @ BBR NPs prepared from 0.2 mg mL<sup>-1</sup> PDA; (I) TEM images of PDA @ BBR NPs prepared from 0.5 mg mL<sup>-1</sup> PDA; (J) UV-visible spectra and (K) fluorescence spectra of BBR and PDA@BBR NPs.

be obtained by prolonging the reaction time or increasing the dopamine concentration. The morphological changes of PDA@BBR NPs with different coating thicknesses were observed (Figure 2G-I). The NPs exhibit uniform spherical shapes, and as the dopamine concentration ( $0.1, 0.2, 0.5 \mu\text{g}\cdot\text{mL}^{-1}$ ) increases, the outer shell becomes more pronounced.

The UV-vis spectra characteristics of BBR NPs and PDA@BBR NPs are shown in Figure 2J. BBR NPs exhibit four distinct characteristic peaks at 227, 263, 345, and 421 nm. In contrast, PDA@BBR NPs show a smooth absorbance curve with weak and unclear peaks at 263 and 345 nm wavelengths, indicating successful dopamine encapsulation. The fluorescence spectrum shows that BBR NPs have an emission peak at 553 nm, which can be attributed to the aggregation-induced emission (AIE) characteristics of BBR<sup>20</sup> (Figure 2K). In contrast, PDA@BBR NPs do not show any obvious emission spectrum, indicating that PDA can shield the optical properties of the internal BBR NPs. The standard curve of the fluorescence spectrum of BBR NPs is represented by the equation  $Y=11.535x+1.7939$  ( $R^2=0.9987$ ) over a linear range of  $0.1\text{--}2.0\mu\text{g}\cdot\text{mL}^{-1}$ . According to this standard curve, the encapsulation efficiency (EE) of PDA@BBR NPs is  $96.2\% \pm 21.6\%$ , with a loading capacity (LC) of  $66.8\% \pm 12.3\%$ .

## Stability of Polydopamine-Coated Berberine Nanoparticles

The hypothesis that coating BBR NPs with PDA can prevent their aggregation was tested. The stability of PDA-coated BBR NPs ( $50 \mu\text{g}\cdot\text{mL}^{-1}$ ) was assessed using DLS. As shown in Figure 3A, the hydrodynamic size of BBR NPs increased from 150 nm to approximately 490 nm within 7 days, indicating a decrease in stability over time. In contrast, the size of PDA@BBR NPs remained relatively constant. The changes in PDI also exhibited a similar trend, as shown in Figure 3B. Additionally, the study found that the zeta potential of BBR NPs ranged from  $-14.7 \text{ mV}$  to  $-5 \text{ mV}$ , while the zeta

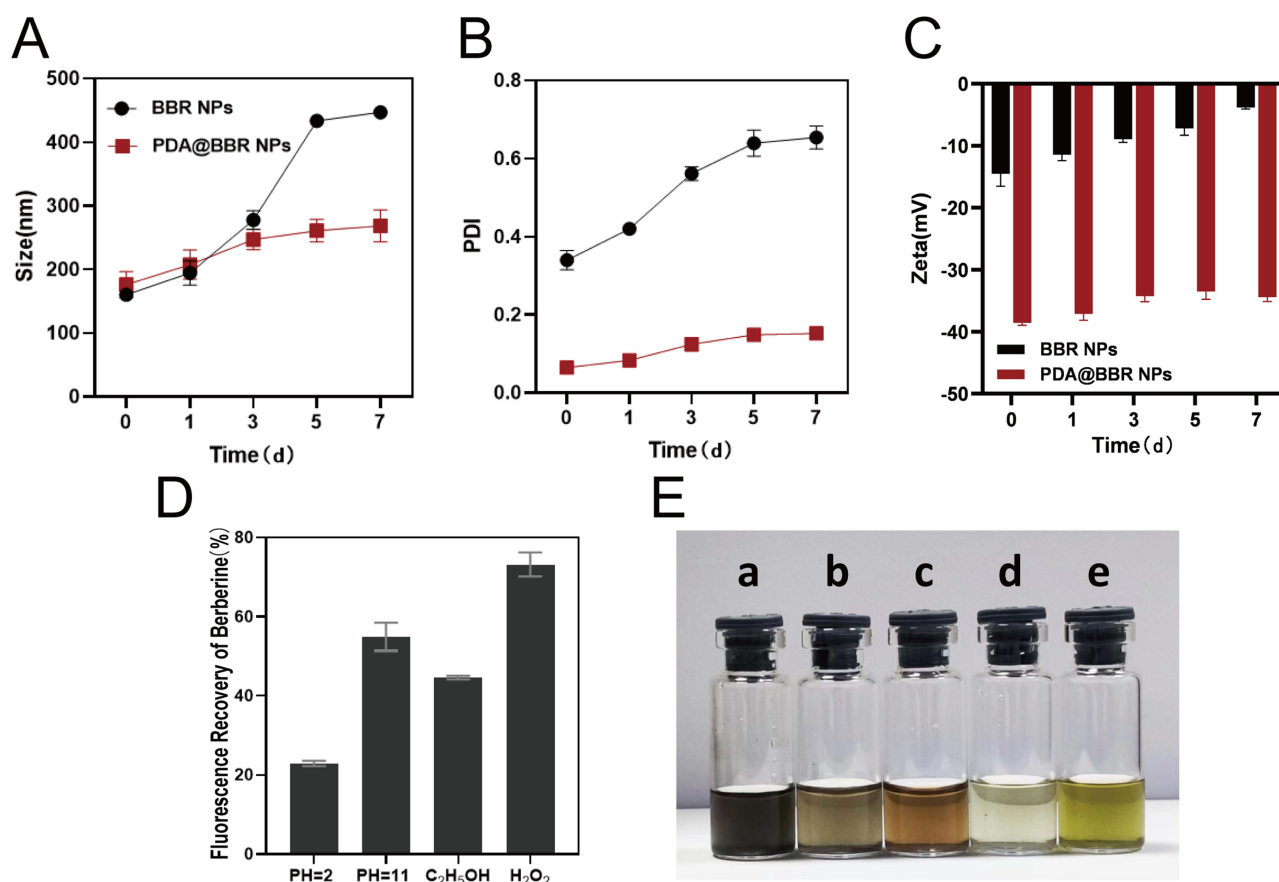


**Figure 3** Stability of BBR NP and PDA@BBR NPs solutions. Changes in (A) particle size, (B) PDI, and (C) zeta potential of BBR NPs and PDA@BBR NPs at 0, 1, 3, 5, and 7 days; (D) Percentage of fluorescence recovery of Berberine for PDA@BBR NPs in different media environments; (E) Appearance of PDA@BBR NPs solutions in different media environments for 24 hours: (a) pure water; (b) pH=2; (c) pH=11; (d) ethanol; and (e) hydrogen peroxide.



potential of PDA@BBR NPs remained relatively stable at around  $-38$  mV (Figure 3C). It is evident that the PDA coating significantly enhances both the stability and uniformity of BBR NPs.

In different media, the damage to the PDA coating or the release of internal drugs from PDA@BBR NPs can be reflected by the fluorescence recovery of BBR. As shown in Figure 3D, PDA@BBR NPs are relatively stable in acidic medium at pH=2, with only 20% of the drug released. Compared to the solution in water, the solution color remains unchanged, but the stability is reduced (Figure 3E). In alkaline medium at pH=11, the drug release rate exceeds 50%, and the solution turns brown. Notably, in hydrogen peroxide medium, the drug release rate surpasses 70%, and the solution turns yellow, indicating significant leakage of BBR.

## ROS-Stimulus Response of Polydopamine-Coated Berberine Nanoparticles

PDA was susceptible to degrade under oxidative conditions, leading to the specific release of internal drugs in the high-level ROS environment. The release behavior of PDA@BBR NPs in response to  $H_2O_2$  (one of the most common endogenous reactive oxygen species) was confirmed through TEM imaging. As shown in Figure 4A, PDA@BBR NPs were initially well dispersed and exhibited a uniform spherical shape. After soaking in  $H_2O_2$  solution for one hour, the outer shell of the nanoparticles became blurred, with a tendency to dissolve. After 6 hours, the nanoparticles began to degrade, resulting in the drug started to partially dissolve. After 24 hours, the polydopamine completely degraded, and a large amount of the drug dissolved. DLS size analysis measurements confirmed the particle size changes observed by TEM. As the PDA layer degraded, the particle size became irregular, and due to the significant release of BBR, formed micrometer-sized aggregates (Figure 4B). Furthermore, the release of BBR from PDA@BBR NPs in 30%  $H_2O_2$  was found to be time-dependent (Figure 4C). Similarly, the release of BBR was dependent on the concentration of  $H_2O_2$ , as demonstrated in Figure 4D. These results indicate that PDA@BBR NPs have ROS-responsive characteristics, making them well-suited for application at inflammatory sites to regulate the release of BBR. Although it is not feasible to regulate the drug release rate by manipulating inflammation levels in vivo, this nanoscale formulation can achieve controlled release of BBR by adjusting the thickness of the PDA coating. Figure 4E illustrates that under 3%  $H_2O_2$  conditions, the thinner the PDA coating, the faster the release rate of BBR.

Furthermore, as shown in Figure 5A, after LPS-induced ROS production in Caco-2 cells, we observed the release of BBR from PDA@BBR NPs in an inflammatory environment using fluorescence microscopy. Under normal in vitro culture conditions, Caco-2 cells could differentiate and formed a complete monolayer of intestinal epithelial cells, exhibiting characteristics of mature epithelial cells. As shown in Figure 5B and 5C, under LPS induction, Caco-2 cells underwent inflammation and oxidative stress, leading to an elevated ROS level. At high ROS levels, BBR from PDA@BBR NPs was progressively released (as indicated by green fluorescence) over time, which was consistent with the results shown in Figure 4, while significant BBR fluorescence was not detected in normal cells.

## In vivo Adhesion of Polydopamine-Coated Berberine Nanoparticles

The adhesion properties of PDA@BBR NPs were investigated using in vivo and ex vivo fluorescence imaging in mice. As shown in Figure 6, 2 hours after oral administration in healthy mice, the free Cy 7.5 dye predominantly accumulated in the liver, with weaker fluorescence observed in the lungs, kidneys, and colon. Over time, the fluorescence signal in the colon intensified, whereas it diminished in other tissues. In contrast, mice administered with Cy 7.5-labeled PDA@BBR NPs displayed significant accumulation in the colon 2 hours after administration, with only a small amount of fluorescence detected in the lungs. The fluorescence intensity in the colon increased over time and remained prominent within 24 hours. No significant changes or distribution were observed in the heart, liver, spleen, and kidneys, suggesting that PDA@BBR NPs were not digested or metabolized by tissues and organs. However, the intestinal fluorescence decreased in UC mice with high ROS levels, leading to the inflammatory degradation of PDA and subsequent drug release. In vivo experiments demonstrated that the PDA coating can prolong the retention time of BBR in the colon through improved adhesion.

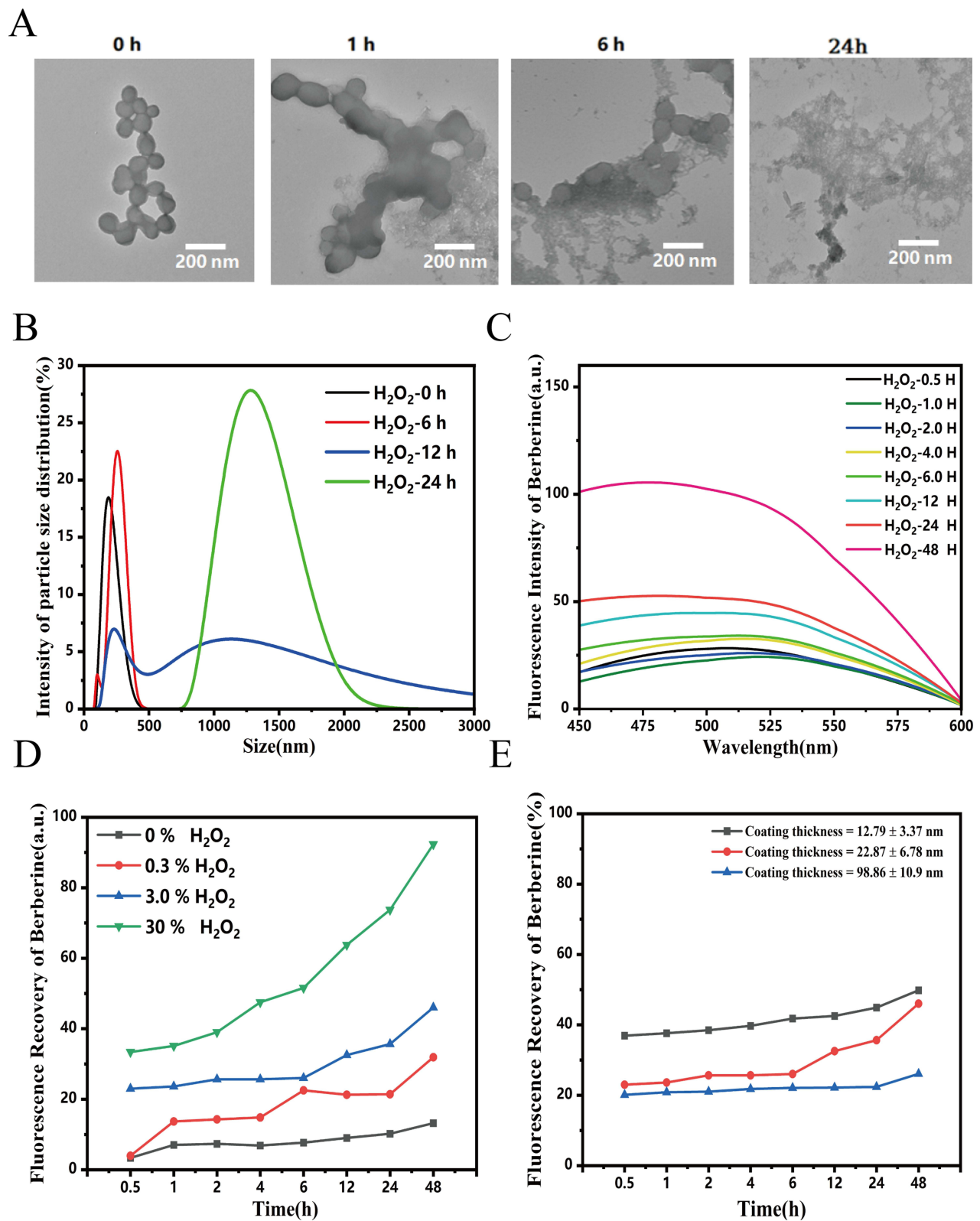


**Figure 4** In vitro ROS stimulation response of PDA@BBR NPs. **(A)** TEM images of PDA@BBR NPs at 0, 6, 12, and 24 h of 3%  $H_2O_2$  stimulation; **(B)** Intensity of particle size distribution of PDA@BBR NPs at 0, 6, 12, and 24 h of 3%  $H_2O_2$  stimulation; **(C)** Fluorescence intensity of Berberine for PDA@BBR under 3%  $H_2O_2$  stimulation at 0.5, 1, 2, 4, 6, 12, 24, and 48 h; **(D)** Effect of different concentrations of  $H_2O_2$  media (0%, 0.3%, 3%, and 30%) on the fluorescence recovery intensity of Berberine for PDA@BBR NPs; **(E)** Effects of different coating thickness on the fluorescence recovery intensity of Berberine for PDA@BBR NPs under 3%  $H_2O_2$  stimulation.

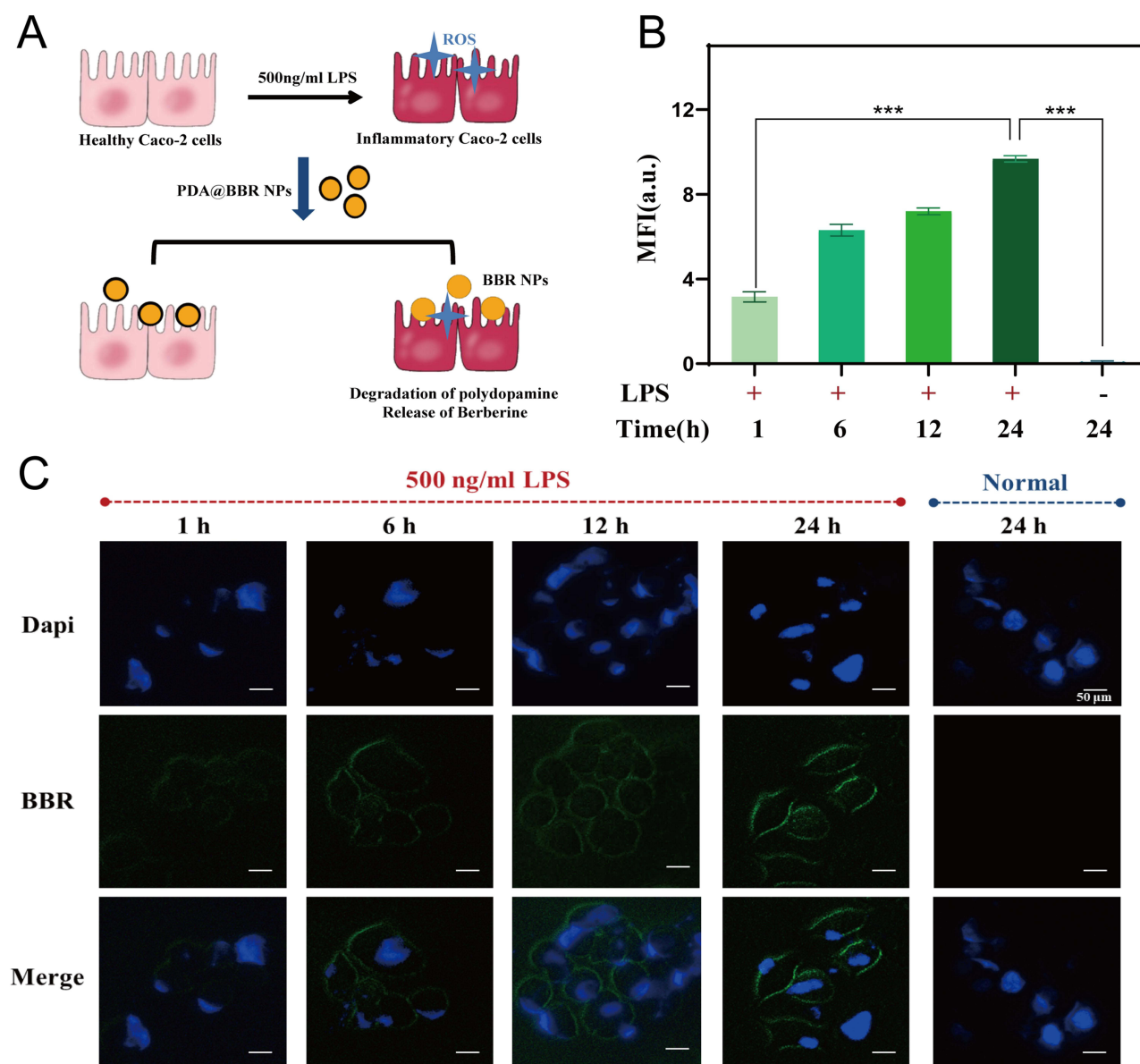


**Figure 5** ROS-responsive release of Berberine for PDA@BBR NPs in Caco-2 cells. **(A)** Schematic diagram of LPS-induced cellular inflammation triggering the release of Berberine for PDA@BBR NPs; **(B)** Fluorescence intensity and **(C)** Fluorescence microscopy images of Berberine released by PDA@BBR NPs in Caco-2 cells at different times. Data are mean  $\pm$  standard deviation ( $n=3$ ) (\*\* $p<0.001$ ).

## In vivo UC Therapeutic Evaluation

In this study, the therapeutic efficacy of PDA@BBR NPs was evaluated using a DSS-induced UC mouse model. The experimental process is shown in Figure 7A. The therapeutic effect of PDA@BBR NPs on UC was evaluated from four aspects: conventional treatment, anti-inflammatory, repair of intestinal mucosal barrier, and immune homeostasis.

### Effect of PDA@BBR NPs on Conventional Therapeutic Indexes in DSS-Induced UC Mice

Weight loss, increased DAI scores, and colon shortening are important indicators of colitis phenotype. As shown in Figure 7B, after DSS induction, the body weight of all groups of mice continued to decrease, but increased after oral administration of free BBR and PDA@BBR NPs. As shown in Figure 7C, compared to the model group ( $8.5 \pm 0.54$ ), oral administration of free BBR ( $5.0 \pm 2.0$ ) and PDA@BBR NPs ( $3.1 \pm 1.5$ ) significantly reduced diarrhea and occult blood. As shown in Figure 7D-G, all treatment groups successfully prevented DSS-induced colon shortening and splenic enlargement, with the PDA@BBR NPs group showing the most significant effect.

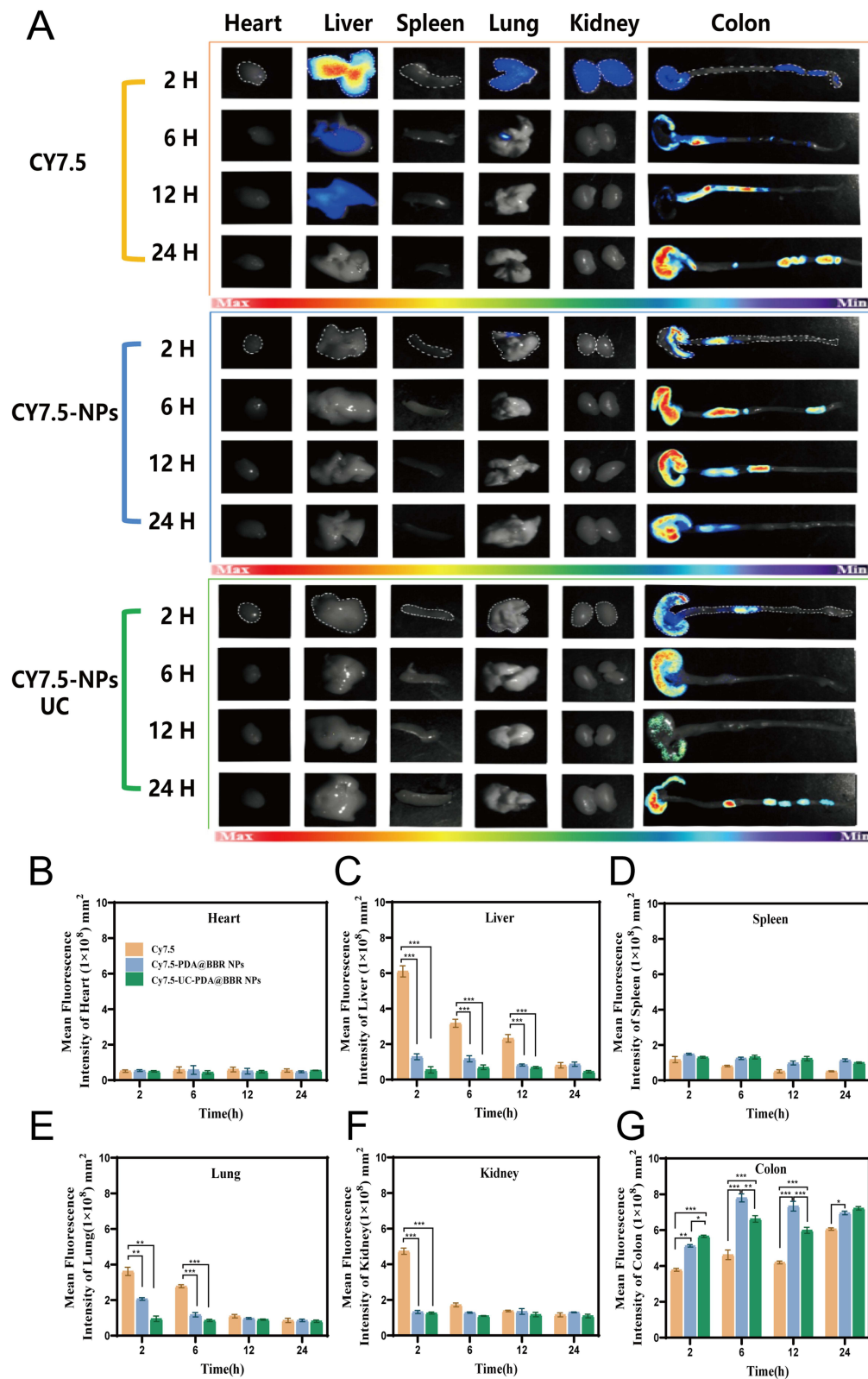


**Figure 6** Adhesion of PDA @ BBR NPs in vitro. **(A)** In vitro fluorescence images at different time points after oral administration of different formulations to mice; **(B-G)** Histogram of fluorescence intensity in each isolated organ of mice from different formulation groups; Data are mean  $\pm$  standard deviation ( $n=3$ ) (\* $p<0.05$ , \*\* $p<0.01$ , \*\*\* $p<0.001$ ).



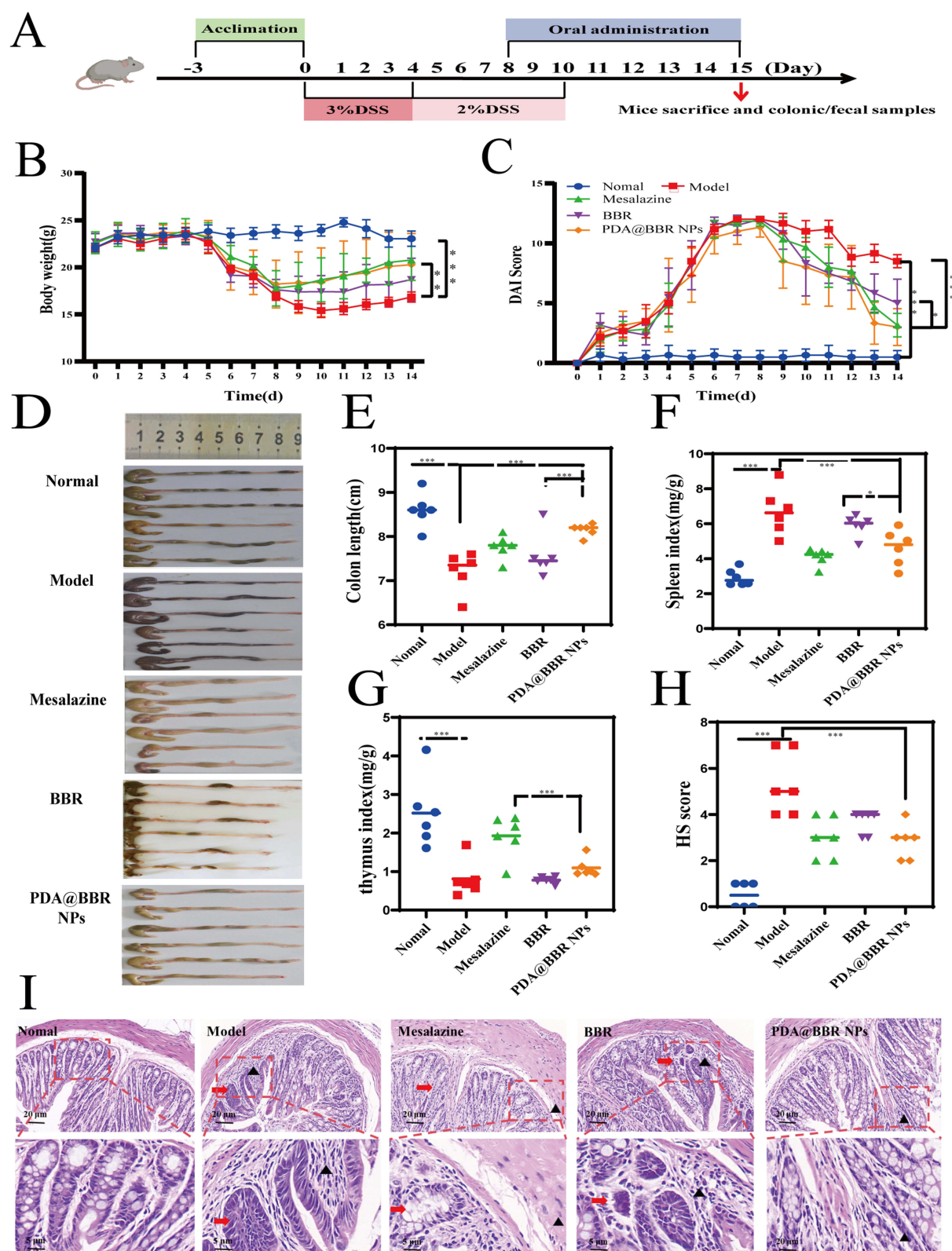


**Figure 7** Examination of in vivo efficacy of BBR NPs and PDA@BBR NPs in the treatment of UC mice. **(A)** Schematic diagram of the construction of UC model and dosing cycle; **(B)** Body weight changes of mice in different groups; **(C)** Changes of DAI score in different groups; **(D)** Photographs of colon appearance of mice in different groups; **(E)** Histogram assessment of colon length of mice in different groups; **(F)** Splenic index assessment and **(G)** thymus index assessment of mice in different groups; **(H)** HS scores of colon sections in different groups; **(I)** HE staining of colon section; Red arrows: absence of epithelial cells or cup cells; Black triangles: aggregation or distribution of inflammatory cells. Data are mean  $\pm$  standard deviation ( $n=6$ ) (\* $p<0.05$ , \*\*\* $p<0.001$ ).



Furthermore, H&E staining and HS scores were used to assess the degree of inflammatory damage in colon tissues. The results in Figure 7H and Figure I showed that the colon HS score of the model group of mice was significantly higher than that of the normal group ( $p < 0.001$ ). The HS score of the PDA@BBR NPs group of mice was significantly lower than that of the model group ( $p < 0.001$ ). In the control group, the mouse colon structure was intact, with clear layers, orderly arranged glands, visible crypts, and goblet cells, with minimal congestion, edema, and inflammatory cell infiltration. The colon crypts and goblet cells of the treatment group mice showed varying degrees of repair and improvement, with a reduction in inflammatory cell infiltration. The colon mucosa of the PDA@BBR NPs group showed minimal aggregation of inflammatory cells, with a morphology similar to that of the normal group, indicating a positive therapeutic effect.

### Effect of PDA@BBR NPs on Colonic Inflammatory Factors in UC Mice

The study found that the severity of inflammation in UC was positively correlated with the levels of pro-inflammatory cytokines in the colon tissue. Therefore, the levels of inflammatory cytokines in the mouse colon were evaluated to determine the therapeutic effect of PDA@BBR NPs.<sup>21–23</sup> As shown in Figure 8A, compared to the normal group, the expression of pro-inflammatory factors TNF- $\alpha$ , IL-6, TGF- $\beta$ , and MPO in the colon tissue of the model group was significantly increased ( $p < 0.01$  or  $p < 0.001$ ). In addition, the expression of the anti-inflammatory factor IL-10 was significantly lower than in the normal group ( $p < 0.001$ ). Conversely, compared to the model group, the expression of TNF- $\alpha$  and MPO in the colon tissue of the PDA@BBR NPs group was significantly reduced ( $p < 0.05$  or  $p < 0.001$ ). Furthermore, the expression of IL-10 in the BBR group was significantly higher than in the model group ( $p < 0.05$ ), and the expression of IL-6 was significantly lower than in the model group ( $p < 0.001$ ). The results indicate that PDA@BBR NPs can prevent the deterioration of UC symptoms by reducing the expression of pro-inflammatory factors and increasing the levels of anti-inflammatory factors in the mouse colon tissue, thereby inhibiting the development of UC symptoms.

### Changes of T-Lymphocyte Subpopulations in the Spleen of Mice

T-lymphocytes play a crucial role in the immune response, and a significant number of CD4<sup>+</sup> T-cells infiltrate the lesion site in subpopulations of UC. CD4<sup>+</sup> T-cells, specifically Th17 and Treg cells, are involved in regulating the autoimmune response.<sup>24,25</sup> To evaluate the impact of PDA@BBR NPs on immune homeostasis, flow cytometry was used to analyze changes in T lymphocyte subsets in mouse spleens. As shown in Figure 8B, compared with the normal group, splenic CD4<sup>+</sup>IL17 levels were elevated ( $p < 0.01$ ) and CD25<sup>+</sup>FOXP3 levels were decreased ( $p < 0.01$ ) in the model group, suggesting the success of membranopoiesis. Additionally, splenic CD4<sup>+</sup>IL17 levels were significantly decreased in mice in the mesalazine group compared with the model group ( $p < 0.01$ ). A similar trend of decrease in CD4<sup>+</sup>IL17 was observed in both the BBR group and the PDA@BBR NPs group compared with the model group. In addition, compared to the model group, splenic CD25<sup>+</sup>FOXP3 levels were significantly higher in mice treated with mesalazine, BBR and PDA@BBR NPs. In conclusion, BBR and PDA@BBR NPs may restore immune function and exert their therapeutic effects on UC by regulating the balance between Th17 cells and Treg cells.

## Discussion

The etiology of UC is complex, and it tends to recur, making it a difficult-to-treat chronic inflammatory gastrointestinal disease. Long-term pathological stimulation of the intestinal mucosa significantly increases the incidence of colon cancer in patients.<sup>26</sup> In recent years, traditional Chinese medicine has increasingly become a popular complementary therapy for some UC patients because of its minimal side effects, good patient tolerance, and the ability to target multiple pathways and points. For example, baicalin can regulate the PI3K/AKT signaling pathway, reduce IL-6, TNF- $\alpha$ , and IL-1 $\beta$ , upregulate IL-10, and promote the expression of tight junction proteins.<sup>27</sup> Puerarin can alleviate UC symptoms by increasing levels of short-chain fatty acids and stimulating mucin secretion.<sup>28</sup> This study also found that berberine could decrease the expression of the pro-inflammatory factor IL-6 and increase the expression of the anti-inflammatory factor IL-10 (Figure 8A), and improve UC conditions by regulating the balance of Th17/Treg cells (Figure 8B). Despite the multi-component and multi-target advantages of traditional Chinese medicine, how to improve the efficient delivery of drugs to the colonic lesions remained an urgent issue to be addressed. In recent years, nanotechnology has shown promise as a new type of colonic targeted drug delivery system for

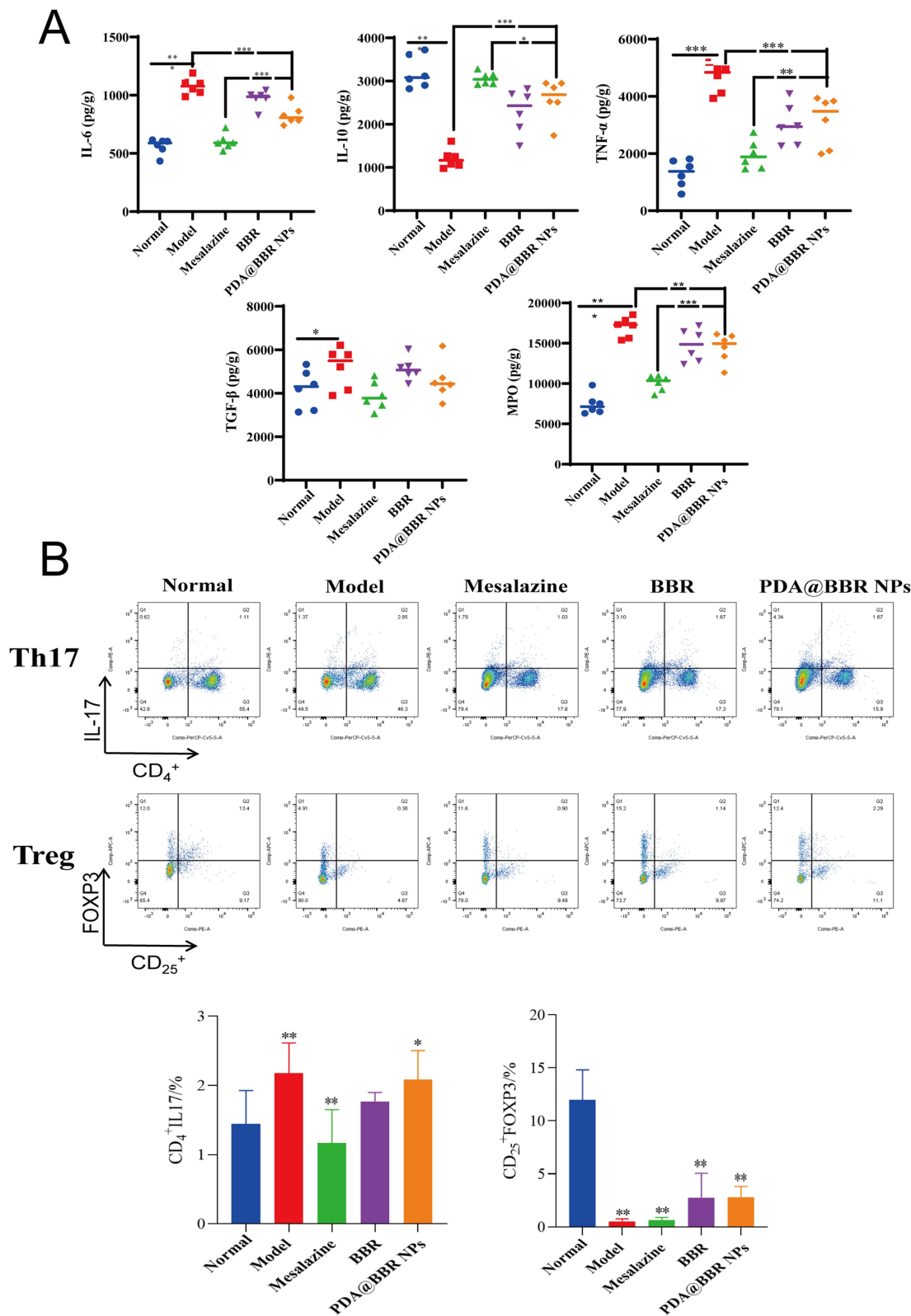


**Figure 8** Anti-inflammatory effects and modulation of immune homeostasis. **(A)** Histogram analysis of changes in colonic IL-6, IL-10, TNF- $\alpha$ , TNF- $\beta$  and MPO by different preparations; **(B)** Changes in T-lymphocyte subpopulations in the spleen of mice; Data are mean  $\pm$  standard deviation (n=6) (\*p<0.05, \*\*p<0.01, \*\*\*p<0.001 vs normal).

the treatment of UC. For example, Raj et al prepared pH-sensitive curcumin nanoparticles using Eudragit EF 30D, achieving a cumulative drug release of up to 84.7% in simulated colonic fluid.<sup>29</sup> Castangia et al used chitosan-alginate calcium microspheres to deliver icariin to the colon via enzyme response.<sup>30</sup> Although these targeted formulations could promote the specific release of drugs, frequent administration was required for efficacy due to the characteristic of recurrent diarrhea in UC. Therefore, the development of a drug delivery system with long-lasting and specific release properties for UC, is urgently needed. In this study, we synthesized nanoparticles with berberine as the core and polydopamine as the shell, achieving the dual effects of “prolonging drug residence time” and “inflammation site-responsive drug release”. This approach reduced the need for patients to repeatedly administer drugs over the long term and prevented the burst release of drugs at the non-inflammatory site.

Research has shown that the intestinal mucus layer of UC patients is damaged, leading to direct contact between intestinal contents and epithelial cells.<sup>31,32</sup> This results in the release of a large amount of ROS, which is 10–100 times high than normal tissues.<sup>33</sup> Achieving targeted and selective drug delivery through abnormally high concentrations of ROS at the site of inflammation can ensure that the drug is released only at the site of intestinal inflammation, not in healthy tissue.<sup>34,35</sup> Literature reports that disulfide bonds have ROS-responsive properties, and using D- $\alpha$ -tocopherol-polyethylene glycol succinate-poly ( $\beta$ -thioester) copolymer (TPGS-PBTE) to deliver luteolin can release luteolin at the lesion site with high ROS expression, helping to alleviate colonic inflammation and protect colonic tissue integrity.<sup>8</sup> Zhang et al developed an intelligent nano-therapy AON (nanoparticles based on  $\beta$ -cyclodextrin 4-phenylboronic acid pinocembrin ester, containing the membrane-degrading protein A1 mimetic peptide Ac2-26), achieving specific release and accumulation of Ac2-26 in the ROS environment.<sup>36</sup> However, the safety of drug carriers and the kinetics of drug release in response to redox stimuli are the main issues of ROS-responsive drug delivery systems. Prodrugs containing thioether bonds are prone to hydrolysis in the bloodstream, while aryl boronic esters produce the intermediate quinone methide (QM) during degradation.<sup>37</sup> Fortunately, more studies have found that dopamine and its derivatives can be used for ROS-responsive systems, exhibiting good biocompatibility and degradability.<sup>38,39</sup> Inspired by these researchers, we employed a straightforward approach to apply a uniform polydopamine coating to the surface of berberine nanoparticles (PDA@BBR NPs) in order to overcome these shortcomings. The successful coating of polydopamine was confirmed through particle size analysis, TEM, and spectral analysis (Figure 2). The polydopamine coating can improve the dispersibility and stability of poorly soluble drug nanoparticles (eg berberine) due to the spatial hindrance effect of the polymer, (Figure 3). Gratifyingly, due to the facile degradation of polydopamine by H<sub>2</sub>O<sub>2</sub>, PDA@BBR NPs can gradually release berberine in a high-ROS environment, facilitating targeted release and accumulation of the drug (Figure 4). At the same time, we established an LPS-induced Caco-2 cell inflammation model. When harmful substances such as LPS invade intestinal epithelial cells, they caused damage to the intestinal epithelial cells, intestinal inflammation, and oxidative stress (excessive levels of ROS).<sup>40</sup> Fluorescence microscopy was used to detect the fluorescence intensity of berberine. The results revealed that in the presence of ROS, the system was able to degrade polydopamine and achieve the slow release of berberine (Figure 5). In comparison to non-targeted berberine lipid carriers,<sup>41</sup> this system can facilitate the slow release of the drug at the site of colonic inflammation, achieving a stable drug concentration at the site and reducing the pathological stimulation of the intestinal mucosa caused by sudden drug release.

To further evaluate the adhesion capabilities of PDA@BBR NPs, we conducted a study on the fluorescence intensity of ex vivo animal organs and quantitatively analyzed them using Image J. On one hand, the catechol functional groups on polydopamine readily adhere to the small intestinal mucosa,<sup>42,43</sup> and the negatively charged PDA@BBR NPs can adhere to the inflamed mucosa via electrostatic adsorption.<sup>44</sup> As a result, PDA@BBR NPs can prolong the drug's residence time in the colon. As shown in Figure 6, strong fluorescence intensity was detected in the colon of normal mice within 24 hours after oral administration of PDA@BBR NPs, compared to the free Cy7.5 dye group. On the other hand, polydopamine itself can act as a ROS-responsive agent and scavenger.<sup>45</sup> Due to the high levels of ROS at the site of colonic inflammation, after oral administration of PDA@BBR NPs in UC mice, polydopamine degradation occurs, resulting in a slight decrease in the drug's fluorescence intensity in the colon. Compared to the polydopamine nanoparticles loaded with xanthatin (PDA-XA NPs) prepared by Zhou et al,<sup>46</sup> the PDA-coated berberine nanoparticles developed in this study have similar adhesion properties and higher ROS responsiveness, making them more suitable for colonic inflammatory diseases. In addition, compared to traditional non-targeted oral formulations, this system can

reduce the frequency of administration by prolonging the drug's residence time, thereby avoiding the side effects and drug resistance caused by repeated administration.

This study utilized the various properties of polydopamine to suggest a responsive drug release at the site of colonic inflammation. This approach also involved adhering the drug to the mucosal surface, thereby extending the drug's residence time. Furthermore, in comparison to nano-delivery systems modified with various materials, this system offers the advantages of simple, safe, and controllable preparation. In this study, a mouse model of dextran sulfate sodium (DSS)-induced ulcerative colitis was used, and treatments with mesalazine,<sup>47</sup> BBR, and PDA@BBR NPs were conducted. The mice exhibited symptoms and pathological characteristics similar to those of chronic UC induced clinically after modeling.<sup>48</sup> After treatment with BBR and PDA@BBR NPs, the symptoms of DSS-induced ulcerative colitis were alleviated, and the pathological tissue examination also showed varying degrees of repair in colonic goblet cells and crypts, with reduced inflammatory cell infiltration.<sup>49</sup> Among these parameters, including changes in mouse body weight, DAI score, and colon length, it was found that PDA@BBR NPs had a more effective therapeutic effect on UC than BBR (Figure 7). Additionally, this study examined the expression of inflammatory factors in the intestinal mucosal cells of mice with DSS-induced ulcerative colitis and its significance. The experimental results showed that PDA@BBR NPs can prevent the progression of UC symptoms by reducing the expression of pro-inflammatory factors in the colonic tissue of mice, increasing anti-inflammatory factors, and balancing Th17/Treg cells. This approach effectively repairs intestinal mucosa and alleviates symptoms of UC, demonstrating a certain therapeutic effect on DSS-induced UC in mice (Figure 8).

## Conclusion

In conclusion, we have successfully developed a novel nanoparticle system with ROS-responsive and long-lasting adhesion properties by coating PDA on BBR nanoparticles. These nanoparticles can enhance the solubility and stability of BBR, as well as promote its retention and release at the site of colonic inflammation. PDA@BBR NPs exhibit effective ROS-responsive release in vitro and significant adhesion properties in vivo. Correspondingly, oral administration of PDA@BBR NPs in UC mice can alleviate colonic inflammation and repair intestinal mucosa. Therefore, PDA@BBR NPs can serve as an excellent nanosystem for the treatment of UC.

## Acknowledgment

We acknowledge the support of experiment center for science and technology at Nanjing University of Chinese Medicine for technical support and Jiangsu key laboratory of Chinese Medicine Processing for experimental support.

## Funding

Supported by National Natural Science Foundation (No. 82074125, 82173992, 82230117).

## Disclosure

Ms Chenqi Chang reports a patent "An antimicrobial drug carrier with ROS response and adhesion and its preparation method" pending to Rui Chen, Chenqi Chang, Yue Liu, Zhipeng Chen. The authors report no other conflicts of interest in this work.

## References

1. Segal JP, LeBlanc JF, Hart AL. Ulcerative colitis: an update. *Clin Med Lond*. 2021;21(2):135–139. doi:10.7861/clinmed.2021-0080
2. Fiorino G, Danese S, Giacobazzi G, Spinelli A. Medical therapy versus surgery in moderate-to-severe ulcerative colitis. *Dig Liver Dis*. 2021;53(4):403–408. doi:10.1016/j.dld.2020.09.022
3. Damião AOMC, de Azevedo MFC, Carlos AS, Wada MY, Silva TVM, Feitosa FC. Conventional therapy for moderate to severe inflammatory bowel disease: a systematic literature review. *World J Gastroenterol*. 2019;25(9):1142–1157. doi:10.3748/wjg.v25.i9.1142
4. Wilson DS, Dalmasso G, Wang L, Sitaraman SV, Merlin D, Murthy N. Orally delivered thioketal nanoparticles loaded with TNF- $\alpha$ -siRNA target inflammation and inhibit gene expression in the intestines. *Nat Mater*. 2010;9(11):923–928. doi:10.1038/nmat2859
5. Yang X, Mao Z, Huang Y, et al. Reductively modified albumin attenuates DSS-Induced mouse colitis through rebalancing systemic redox state. *Redox Biol*. 2021;41:101881. doi:10.1016/j.redox.2021.101881
6. Nguyen TT, Trinh NT, Tran HN, et al. Improving silymarin oral bioavailability using silica-installed redox nanoparticle to suppress inflammatory bowel disease. *J Control Release*. 2021;331:515–524. doi:10.1016/j.jconrel.2020.10.042

7. Huang C, Xu J, Li J, et al. Hydrogen peroxide responsive covalent cyclodextrin framework for targeted therapy of inflammatory bowel disease. *Carbohydr Polym.* **2022**;285:119252. doi:10.1016/j.carbpol.2022.119252
8. Tan C, Fan H, Ding J, et al. ROS-responsive nanoparticles for oral delivery of luteolin and targeted therapy of ulcerative colitis by regulating pathological microenvironment. *Mater Today Bio.* **2022**;14:100246. doi:10.1016/j.mtbo.2022.100246
9. Zhao P, Xia X, Xu X, et al. Nanoparticle-assembled bioadhesive coacervate coating with prolonged gastrointestinal retention for inflammatory bowel disease therapy. *Nat Commun.* **2021**;12(1):7162. doi:10.1038/s41467-021-27463-6
10. Xue B, Gu J, Li L, et al. Hydrogel tapes for fault-tolerant strong wet adhesion. *Nat Commun.* **2021**;12(1):7156. doi:10.1038/s41467-021-27529-5
11. Newland B, Wolff P, Zhou D, et al. Synthesis of ROS scavenging microspheres from a dopamine containing poly( $\beta$ -amino ester) for applications for neurodegenerative disorders. *Biomater Sci.* **2016**;4(3):400–404. doi:10.1039/c5bm00542f
12. Hu H, Yang J, Zhong Y, et al. Polydopamine-Pd nanozymes as potent ROS scavengers in combination with near-infrared irradiation for osteoarthritis treatment. *iScience.* **2023**;26(5):106605. doi:10.1016/j.isci.2023.106605
13. Hussain M, Suo H, Xie Y, et al. Dopamine-Substituted Multidomain Peptide Hydrogel with Inherent Antimicrobial Activity and Antioxidant Capability for Infected Wound Healing. *ACS Appl Mater Interfaces.* **2021**;13(25):29380–29391. doi:10.1021/acsami.1c07656
14. Habtemariam S. Berberine and inflammatory bowel disease: a concise review. *Pharmacol Res.* **2016**;113(Pt A):592–599. doi:10.1016/j.phrs.2016.09.041
15. Liu SC, Lee HP, Hung CY, Tsai CH, Li TM, Tang CH. Berberine attenuates CCN2-induced IL-1 $\beta$  expression and prevents cartilage degradation in a rat model of osteoarthritis. *Toxicol Appl Pharmacol.* **2015**;289(1):20–29. doi:10.1016/j.taap.2015.08.020
16. Cheng F, Wang Y, Li J, et al. Berberine improves endothelial function by reducing endothelial microparticles-mediated oxidative stress in humans. *Int J Cardiol.* **2013**;167(3):936–942. doi:10.1016/j.ijcard.2012.03.090
17. Bonamassa B, Moschetta A. Atherosclerosis: lessons from LXR and the intestine. *Trends Endocrinol Metab.* **2013**;24(3):120–128. doi:10.1016/j.tem.2012.10.004
18. Sham HP, Bazett M, Bosiljcic M, et al. Immune Stimulation Using a Gut Microbe-Based Immunotherapy Reduces Disease Pathology and Improves Barrier Function in Ulcerative Colitis. *Front Immunol.* **2018**;9:2211. doi:10.3389/fimmu.2018.02211
19. Lee H, Dellatore SM, Miller WM, Messersmith PB. Mussel-inspired surface chemistry for multifunctional coatings. *Science.* **2007**;318(5849):426–430. doi:10.1126/science.1147241
20. Gu Y, Zhao Z, Su H, et al. Exploration of biocompatible AIEgens from natural resources. *Chem Sci.* **2018**;9(31):6497–6502. doi:10.1039/c8sc01635f
21. Lu PD, Zhao YH. Targeting NF- $\kappa$ B pathway for treating ulcerative colitis: comprehensive regulatory characteristics of Chinese medicines. *Chin Med.* **2020**;15:15. doi:10.1186/s13020-020-0296-z
22. Zhu L, Gu P, Shen H. Protective effects of berberine hydrochloride on DSS-induced ulcerative colitis in rats. *Int Immunopharmacol.* **2019**;68:242–251. doi:10.1016/j.intimp.2018.12.036
23. Yao D, Dong M, Dai C, Wu S. Inflammation and Inflammatory Cytokine Contribute to the Initiation and Development of Ulcerative Colitis and Its Associated Cancer. *Inflamm Bowel Dis.* **2019**;25(10):1595–1602. doi:10.1093/ibd/izz149
24. Gui X, Li J, Ueno A, Iacucci M, Qian J, Ghosh S. Histopathological Features of Inflammatory Bowel Disease are Associated With Different CD4+ T Cell Subsets in Colonic Mucosal Lamina Propria. *J Crohns Colitis.* **2018**;12(12):1448–1458. doi:10.1093/ecco-jcc/jjy116
25. Guo J, Zhang YY, Sun M, Xu LF. Therapeutic Potential of Curcumin in a Rat Model of Dextran Sulfate Sodium-Induced Ulcerative Colitis by Regulating the Balance of Treg/Th17 Cells. *Inflammation.* **2022**;45(6):2163–2171. doi:10.1007/s10753-022-01678-1
26. Shah SC, Itzkowitz SH. Colorectal Cancer in Inflammatory Bowel Disease: mechanisms and Management. *Gastroenterology.* **2022**;162(3):715–730.e3. doi:10.1053/j.gastro.2021.10.035
27. Zhu L, Shen H, Gu PQ, Liu YJ, Zhang L, Cheng JF. Baicalin alleviates TNBS-induced colitis by inhibiting PI3K/AKT pathway activation. *Exp Ther Med.* **2020**;20(1):581–590. doi:10.3892/etm.2020.8718
28. Wu Y, Li Y, Ruan Z, et al. Puerarin Rebuilding the Mucus Layer and Regulating Mucin-Utilizing Bacteria to Relieve Ulcerative Colitis. *J Agric Food Chem.* **2020**;68(41):11402–11411. doi:10.1021/acs.jafc.0c04119
29. Raj PM, Raj R, Kaul A, Mishra AK, Ram A. Biodistribution and targeting potential assessment of mucoadhesive chitosan nanoparticles designed for ulcerative colitis via scintigraphy. *RSC Adv.* **2018**;8(37):20809–20821. doi:10.1039/c8ra01898g
30. Castangia I, Năcher A, Caddeo C, et al. Therapeutic efficacy of quercetin enzyme-responsive nanovesicles for the treatment of experimental colitis in rats. *Acta Biomater.* **2015**;13:216–227. doi:10.1016/j.actbio.2014.11.017
31. Johansson ME, Gustafsson JK, Holmén-Larsson J, et al. Bacteria penetrate the normally impenetrable inner colon mucus layer in both murine colitis models and patients with ulcerative colitis. *Gut.* **2014**;63(2):281–291. doi:10.1136/gutjnl-2012-303207
32. Pelaseyed T, Bergström JH, Gustafsson JK, et al. The mucus and mucins of the goblet cells and enterocytes provide the first defense line of the gastrointestinal tract and interact with the immune system. *Immunol Rev.* **2014**;260(1):8–20. doi:10.1111/imr.12182
33. Tian T, Wang Z, Zhang J. Pathomechanisms of Oxidative Stress in Inflammatory Bowel Disease and Potential Antioxidant Therapies. *Oxid Med Cell Longev.* **2017**;2017:4535194. doi:10.1155/2017/4535194
34. Li S, Wu T, Wu J, et al. Cyclosporine A-Encapsulated pH/ROS Dual-Responsive Nanoformulations for the Targeted Treatment of Colitis in Mice. *ACS Biomater Sci Eng.* **2023**;9(10):5737–5746. doi:10.1021/acsbmaterials.3c01191
35. Wang Y, Wang X, Lv Y, et al. A ROS-responsive fluorescent probe detecting experimental colitis by functional polymeric nanoparticles. *Int J Pharm.* **2021**;609:121125. doi:10.1016/j.ijpharm.2021.121125
36. Li C, Zhao Y, Cheng J, et al. A Proresolving Peptide Nanotherapy for Site-Specific Treatment of Inflammatory Bowel Disease by Regulating Proinflammatory Microenvironment and Gut Microbiota. *Adv Sci.* **2019**;6(18):1900610. doi:10.1002/advs.201900610
37. Han GS, Domaille DW. Connecting the dynamics and reactivity of arylboronic acids to emergent and stimuli-responsive material properties. *J Mater Chem B.* **2022**;10(33):6263–6278. doi:10.1039/d2tb00968d
38. Song Y, Cai L, Tian Z, Wu Y, Chen J. Phytochemical Curcumin-Coformulated, Silver-Decorated Melanin-like Polydopamine/Mesoporous Silica Composites with Improved Antibacterial and Chemotherapeutic Effects against Drug-Resistant Cancer Cells. *ACS Omega.* **2020**;5(25):15083–15094. doi:10.1021/acsomega.0c00912
39. Wu H, Wei M, Xu Y, et al. PDA-Based Drug Delivery Nanosystems: a Potential Approach for Glioma Treatment. *Int J Nanomed.* **2022**;17:3751–3775. doi:10.2147/IJN.S378217



40. Du L, Li J, Zhang X, et al. Pomegranate peel polyphenols inhibits inflammation in LPS-induced RAW264.7 macrophages via the suppression of TLR4/NF- $\kappa$ B pathway activation. *Food Nutr Res.* 2019;63:10.29219/fnr.v63.3392. doi:10.29219/fnr.v63.3392
41. Deng J, Wu Z, Zhao Z, et al. Berberine-Loaded Nanostructured Lipid Carriers Enhance the Treatment of Ulcerative Colitis. *Int J Nanomed.* 2020;15:3937–3951. doi:10.2147/IJN.S247406
42. Pu Y, Zhu Y, Qiao Z, et al. A Gd-doped polydopamine (PDA)-based theranostic nanoplatfrom as a strong MR/PA dual-modal imaging agent for PTT/PDT synergistic therapy. *J Mater Chem B.* 2021;9(7):1846–1857. doi:10.1039/d0tb02725a
43. Batul R, Tamanna T, Khaliq A, Yu A. Recent progress in the biomedical applications of polydopamine nanostructures. *Biomater Sci.* 2017;5(7):1204–1229. doi:10.1039/c7bm00187h
44. Yang J, Zhou J, Zhao Y, Zhu L, Luo G, Ge B. Hollow CeO<sub>2</sub> with ROS-Scavenging Activity to Alleviate Colitis in Mice. *Int J Nanomed.* 2021;16:6889–6904. doi:10.2147/IJN.S317261
45. Guan H, Xu Z, Du G, et al. A mesoporous polydopamine-derived nanomedicine for targeted and synergistic treatment of inflammatory bowel disease by pH-Responsive drug release and ROS scavenging. *Mater Today Bio.* 2023;19:100610. doi:10.1016/j.mtbio.2023.100610
46. Zhou Y, Zhu X, Lin S, et al. A Novel Nanoparticle Preparation to Enhance the Gastric Adhesion and Bioavailability of Xanthatin. *Int J Nanomed.* 2020;15:5073–5082. doi:10.2147/IJN.S252049
47. Paridaens K, Fullarton JR, Travis SPL. Efficacy of oral prolonged-release mesalazine in moderately active ulcerative colitis. *JGH Open.* 2023;7(7):516–519. doi:10.1002/jgh3.12935
48. Zhou Y, Ji G, Yang X, Chen Z, Zhou L. Behavioral abnormalities in C57BL/6 mice with chronic ulcerative colitis induced by DSS. *BMC Gastroenterol.* 2023;23(1):84. doi:10.1186/s12876-023-02718-2
49. Ungaro R, Mehandru S, Allen PB, Peyrin-Biroulet L, Colombel JF. Ulcerative colitis. *Lancet.* 2017;389(10080):1756–1770. doi:10.1016/S0140-6736(16)32126-2

## International Journal of Nanomedicine

Dovepress

### Publish your work in this journal

The International Journal of Nanomedicine is an international, peer-reviewed journal focusing on the application of nanotechnology in diagnostics, therapeutics, and drug delivery systems throughout the biomedical field. This journal is indexed on PubMed Central, MedLine, CAS, SciSearch®, Current Contents®/Clinical Medicine, Journal Citation Reports/Science Edition, EMBase, Scopus and the Elsevier Bibliographic databases. The manuscript management system is completely online and includes a very quick and fair peer-review system, which is all easy to use. Visit <http://www.dovepress.com/testimonials.php> to read real quotes from published authors.

Submit your manuscript here: <https://www.dovepress.com/international-journal-of-nanomedicine-journal>